Journal of Southeast University (English Edition) Vol. 28, No. 1, pp. 29 - 34 Mar. 2012 ISSN 1003—7985

A novel algorithm of normal attitude regulation for the designed end-effector of a flexible drilling robot

Zhang Laixi Wang Xingsong

(School of Mechanical Engineering, Southeast University, Nanjing 211189, China)

Abstract: An end-effector for a flexible drilling robot is designed, and a novel four-point algorithm of normal attitude regulation for this end-effector is presented. Four non-coplanar points can define a unique sphere tangent to them in spatial geometry, and the center point of the sphere and the radius can be calculated. The shape of a workpiece surface in the machining area is approximately regarded as such a sphere. A vector from the machining point to the center point is thus approximately regarded as a normal vector to the workpiece surface. By this principle, the algorithm first measures four coordinates on the curve in the drilling region using four sensors and calculates the normal vector at the drilling point, then calculates the error between the normal vector and the axis of the spindle. According to this error, the algorithm further figures out the angles of two revolving axes on the end-effector and the displacements of three linear axes on the robot main body, thus it implements the function of adjusting the spindle to be perpendicular to the curve at the drilling point. Simulation results of two kinds of curved surfaces show that accuracy and efficiency can be realized using the proposed algorithm.

Key words: four-point position regulation; end-effector; flexible drilling robot; drilling machining on curved surface

doi: 10.3969/j.issn.1003 - 7985.2012.01.006

With the increasing applications of automation, digitization and modularization technology, higher demands for quality improvement, cost reduction and ergonomic improvement in aircraft fabrication and assembly are required. It is of great significance to machine or fabricate components accurately with drilling machinery in fabrication, assembly and other aspects, so automatic drilling machining technology has become an important application and research direction[1-2]. Automatic drilling equipment widely used in aircraft fabrication and assembly offers an ability to machine or assemble very sophisticated parts, but this depends on high structural stiffness along with very accurate controls to meet with the requirements of desired manufacturing precisions and tolerances. Nevertheless, these kinds of equipment are typically customized for specific requirements of aircraft structure or special users, and such features result in poor universal application, greater size, higher stiffness and higher costs [3-5]. The applications of the equipment are limited in cases such as large size workpiece machining or small workspace for fabrication and assembly, so that some parts cannot but be restricted to be assembled manually which drive costs even higher. And, more importantly, it will cause low connecting quality that can shorten fatigue life due to manual operation with low drilling quality. Meanwhile, manual mistakes can also result in expensive repairs, scrapped parts and schedule delays[6].

The application of automatic drilling technology has been an important research field in flexible aircraft assembly. Huge automatic drilling equipment typically uses the method that the workpiece is regulated while it is anchored. By contrast, an automatic drilling robot typically uses an inverse method so that it can drill machine efficiently and accurately with high flexibility and adaptability. Thus, the application of the automatic drilling robot has been widely researched[7]. The end-effector is the key part of a flexible drilling robot in implementing flexibility which can be installed on not only flexible tracks[6, 8] but also a general industrial robot[9].

Qin et al. [10] presented a three-point bracket regulation algorithm for drilling and riveting of aerofoil. The algorithm used three points near a drilling point to represent the position and orientation of the workpiece, and it then calculated the displacement increment of every kinematics pair by the coordinate transformations determined by the geometrical structure of the drilling system. However, the drilling and riveting equipment was anchored but the workpiece was regulated by using this algorithm. Meanwhile, this algorithm simplified the curve surface of the drilling area into a plane resulting in an increase in measurement errors to some extent. The normal reorientation algorithm in which the workpiece is anchored while the drilling robot regulated has not been widely researched. This paper presents a new four-point algorithm of the normal position and orientation regulation that characterize the curve surface of a workpiece by a sphere rather than by a simplified plane. The calculation and simulation results of two kinds of curve surfaces show that the algorithm is efficient, universal and accurate in practical use.

Received 2011-06-10.

Biographies: Zhang Laixi (1973—), male, graduate; Wang Xingsong (corresponding author), male, doctor, professor, xswang@seu.edu.cn.

Foundation item: National Science and Technology Major Project (No. 2009ZX04014-023).

Citation: Zhang Laixi, Wang Xingsong. A novel algorithm of normal attitude regulation for the designed end-effector of a flexible drilling robot [J]. Journal of Southeast University (English Edition), 2012, 28(1): 29 - 34. [doi: 10.3969/j.issn.1003 - 7985.2012.01.006]

1 Designed End-Effector and Reorientation Principle

As shown in Fig. 1, the designed end-effector consists of the spindle unit, the drive feed unit, the tight unit, the reorientation unit and the support unit. The tight unit applies a preload to the workpiece surface with a force to minimize the systemic vibrations during drilling and to eliminate the gaps in the laminated materials so that the stress concentration caused by the scraps and burrs between the gaps is prevented[7]. The reorientation unit uses four displacement sensors evenly arranged around the spindle to measure the vector normal to the workpiece surface at the drilling point. It comprises two axes which are vertical to each other to drive the spindle to coincide with the normal vector. The support unit connects and supports the other units and fixes the end-effector to a pair of tracks or an industrial robot.

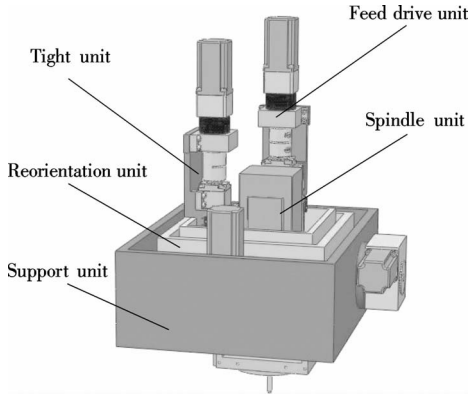

Fig. 1 The end-effector

A kinematics model of the position regulation and the defined coordinate systems of a flexible drilling robot are shown in Fig. 2. The position regulation unit of the robots main body has 3 DOFs for rectilinear motions along the x, y and z axes, respectively, and the end-effector can be free to adjust the spindle's angle within a certain range by using 2-DOFs rotational motions rotating respectively along two axes which are perpendicular to each other.

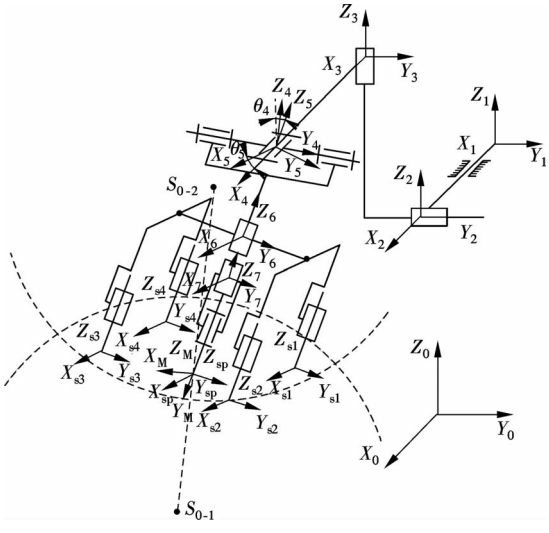

Fig. 2 Mechanical model and coordinate systems of the flexible drilling robot

The defined frames of the flexible drilling robot in Fig. 2 are described as follows:

{0} is the base frame;
{1} to {3}are the robot main body frames;
{4} is the end-effector x axis frame;
{5} is the end-effector y axis frame;
{6} is the end-effector z axis frame;
{7} is the spindle feeder frame;
{s1} to {s4}are the displacement sensors frames;
{sp} is the spindle frame;
{M} is the normal vector frame.

Four non-coplanar points in three-dimensional space can define a unique sphere which is tangential to them. We can calculate the center point of the sphere and the radius and approximately regard the shape of the workpiece surface in the machining area as the sphere. By this principle, the algorithm first measures and calculates the coordinates of four points in the base frame {0} by four displacement sensors evenly arranged around the spindle, and then calculates the center point and the radius of a sphere tangential to the points. The vector from the drilling point to the center point can represent the normal vector to the drilling region because this vector is always normal to the sphere as shown in Fig. 3. However, two conditions are provided so as to make the surface normal measurement method meet the needs of efficiency and accuracy. The first one is that the surface within the four measurement points must be a convex body; i. e., the line between each pair of points on the geometry is inside the geometry. The other one is that the four points must be non-coplanar. If the four points are coplanar, we need rearrange the four sensors to make them non-coplanar, which will be explained in detail later. The rotation angles of the two axes of the normal orientation regulation unit are further calculated and the reorientation completes. However, in this process, the coordinate of the spindle head position has changed due to the displacements of the spindle head. Thus we also need to calculate the displacements of the robot main body along the three

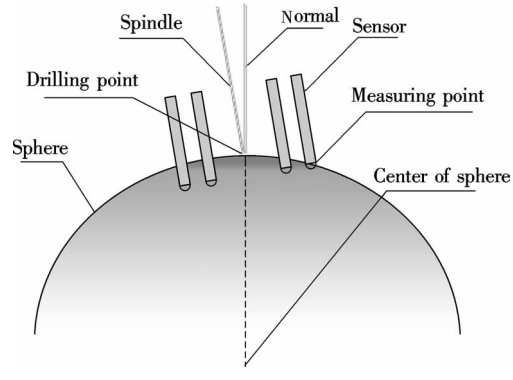

Fig. 3 Principle of normal vector measurement at drilling point

linear axes and remove the spindle to the drilling point again.

2 Reorientation Algorithm

According to the definition of the frames as shown in Fig. 2, the transformation matrix from the sensor coordinate frames $\{si\}$ $(i = 1, 2, 3, 4)$ to the base coordinate frame $\{0\}$ is calculated as

$$
{}^{0}_{si}\boldsymbol{T} = \begin{bmatrix} c5 & 0 & s5 & (z_{si}+z_6)s5+x_1+x_2+x_3+x_4 \\ s4s5 & c4 & -s4c5 & -(z_{si}+z_6)s4c5+y_1+y_2+y_3+y_4 \\ -c4s5 & s4 & c4c5 & (z_{si}+z_6)c4c5+z_1+z_2+z_3+z_4 \\ 0 & 0 & 0 & 1 \end{bmatrix} \tag{1}
$$

The transformation matrix from the end-effector coordinate frame $\{sp\}$ to the base coordinate frame $\{0\}$ are then calculated as

$$
{}^{0}_{sp}\boldsymbol{T} = \begin{bmatrix} c5 & 0 & s5 & (z_{sp}+z_7)s5+x_1+x_2+x_3+x_4 \\ s4s5 & c4 & -s4c5 & -(z_{sp}+z_7)s4c5+y_1+y_2+y_3+y_4 \\ -c4s5 & s4 & c4c5 & (z_{sp}+z_7)c4c5+z_1+z_2+z_3+z_4 \\ 0 & 0 & 0 & 1 \end{bmatrix} \tag{2}
$$

where $c4$ is short for $\cos\theta_4$ and $s4$ for $\sin\theta_4$, and θ_4 and θ_5 are the rotation angles of the normal orientation regulation unit. The following is the same.

The coordinates of the four displacement sensors in the displacement sensors frames $\{si\}$ are ${}^{si}\boldsymbol{S}_i = [0 \quad 0 \quad 0]^{\mathrm{T}}$ $(i = 1, 2, 3, 4)$ and we can obtain them in the base frame by the transformation matrix ${}^{0}_{si}\boldsymbol{T}$ as

$$
{}^{0}\boldsymbol{S}_i = \begin{bmatrix} s_{xi} \\ s_{yi} \\ s_{zi} \end{bmatrix} = \begin{bmatrix} (z_{si}+z_6)s5'+x'_1+x_2+x_3+x_4 \\ -(z_{si}+z_6)s4'c5'+y_1+y'_2+y_3+y_4 \\ (z_{si}+z_6)c4'c5'+z_1+z_2+z'_3+z_4 \end{bmatrix} \tag{3}
$$

where the symbols with apostrophes indicate the original position of every axis before regulation. The algorithm can calculate new angles and displacements based on the original ones to drive the spindle to coincide with the normal vector.

It is assumed that the radius of the sphere determined by the four points is r and the sphere center point is

$$
{}^{0}\boldsymbol{S}_0 = [s_{x0} \quad s_{y0} \quad s_{z0}]^{\mathrm{T}}
$$

Hence, we obtain

$$
\sqrt{(s_{xi}-s_{x0})^2+(s_{yi}-s_{y0})^2+(s_{zi}-s_{z0})^2} = r \qquad i = 1, 2, 3, 4 \tag{4}
$$

Therefore, the sphere center point ${}^{0}\boldsymbol{S}_0$ can be expressed as

$$
\begin{aligned}
s_{x0} &= \frac{1}{2}\frac{(a_{13}m_{14}-a_{14}m_{13})n_{12}+(a_{14}m_{12}-a_{12}m_{14})n_{13}+(a_{12}m_{13}-a_{13}m_{12})n_{14}}{(l_{13}m_{14}-l_{14}m_{13})n_{12}+(l_{14}m_{12}-l_{12}m_{14})n_{13}+(l_{12}m_{13}-l_{13}m_{12})n_{14}} \\
s_{y0} &= \frac{1}{2}\frac{(a_{14}l_{13}-a_{13}l_{14})n_{12}+(a_{12}l_{14}-a_{14}l_{12})n_{13}+(a_{13}l_{12}-a_{12}l_{13})n_{14}}{(l_{13}m_{14}-l_{14}m_{13})n_{12}+(l_{14}m_{12}-l_{12}m_{14})n_{13}+(l_{12}m_{13}-l_{13}m_{12})n_{14}} \\
s_{z0} &= \frac{1}{2}\frac{(a_{13}l_{14}-a_{14}l_{13})m_{12}+(a_{14}l_{12}-a_{12}l_{14})m_{13}+(a_{12}l_{13}-a_{13}l_{12})m_{14}}{(l_{13}m_{14}-l_{14}m_{13})n_{12}+(l_{14}m_{12}-l_{12}m_{14})n_{13}+(l_{12}m_{13}-l_{13}m_{12})n_{14}}
\end{aligned} \tag{5}
$$

where

$$
l_{ij} = s_{xi}-s_{xj},\ m_{ij} = s_{yi}-s_{yj},\ n_{ij} = s_{zi}-s_{zj}
$$
$$
a_{ij} = (s_{xi}^2-s_{xj}^2)+(s_{yi}^2-s_{yj}^2)+(s_{zi}^2-s_{zj}^2)
$$

The solution of the equation set has three kinds of different conditions:

1) There is no solution if the four points are not concyclic but coplanar;

2) There are multiple solutions if the four points are concyclic;

3) There is a unique solution if the four points are non-coplanar.

This paper adopts a method of rearranging the sensors in order to make the four points be non-coplanar in the conditions of 1) and 2) so that Eq. (4) always has a unique solution and the algorithm has generality.

The drilling point is ${}^{0}\boldsymbol{D} = [d_x \quad d_y \quad d_z]^{\mathrm{T}}$ in the base frame. A vector ${}^{0}\boldsymbol{N}$ from ${}^{0}\boldsymbol{D}$ to ${}^{0}\boldsymbol{S}_0$ can be considered as a vector normal to the curve surface at the drilling point.

$$
{}^{0}\boldsymbol{N} = [d_x-s_{x0} \quad d_y-s_{y0} \quad d_z-s_{z0}]
$$

The unit vector of ${}^{0}\boldsymbol{N}$ is expressed as

$$
{}^{0}\boldsymbol{N}_e = [e_x \quad e_y \quad e_z]^{\mathrm{T}} = \frac{[d_x-s_{x0} \quad d_y-s_{y0} \quad d_z-s_{z0}]^{\mathrm{T}}}{\sqrt{(d_x-s_{x0})^2+(d_y-s_{y0})^2+(d_z-s_{z0})^2}} \tag{6}
$$

The z axis of the normal vector frame should coincide with ${}^{0}\boldsymbol{N}_e$. The normal vector frame can also be considered as a frame $\{M\}$ which is rotated relative to the base frame $\{0\}$ about some vector ${}^{0}\boldsymbol{K}$ by angle θ. Then,

$$
{}^{0}\boldsymbol{K} = \begin{bmatrix} 0 \\ 0 \\ 1 \end{bmatrix} \times \begin{bmatrix} e_x \\ e_y \\ e_z \end{bmatrix} = \begin{bmatrix} -e_y \\ e_x \\ 0 \end{bmatrix} \tag{7}
$$

If ${}^{0}\boldsymbol{K} = [k_x \quad k_y \quad k_z]^{\mathrm{T}}$, the rotation matrix can be expressed as [11]

$$\boldsymbol{R}_K(\theta) = \begin{bmatrix} k_x k_x v\theta + c\theta & k_x k_y v\theta - k_z s\theta & k_x k_z v\theta + k_y s\theta \\ k_x k_y v\theta + k_z s\theta & k_y k_y v\theta + c\theta & k_y k_z v\theta - k_x s\theta \\ k_x k_z v\theta - k_y s\theta & k_y k_z v\theta + k_x s\theta & k_z k_z v\theta + c\theta \end{bmatrix} \tag{8}$$

where $v\theta$ is short for $1 - \cos\theta$, and the following is the same.

Combining Eqs. (7) and (8), we obtain

$$\boldsymbol{R}_K(\theta) = \begin{bmatrix} e_y^2 v\theta + c\theta & -e_x e_y v\theta & e_x s\theta \\ -e_x e_y v\theta & e_x^2 v\theta + c\theta & e_y s\theta \\ -e_x s\theta & -e_y s\theta & c\theta \end{bmatrix} \tag{9}$$

Most notably, the following equations can be obtained.

$$\cos\theta = e_z,\ \sin\theta = \sqrt{1 - e_z^2},\ 1 - \cos\theta = 1 - e_z \tag{10}$$

From Eqs. (9) and (10), we can obtain the transformation matrix from frame {M} to frame {0},

$${}^{0}_{\mathrm{M}}\boldsymbol{T} = \begin{bmatrix} e_y^2 v\theta + c\theta & -e_x e_y v\theta & e_x s\theta & d_x \\ -e_x e_y v\theta & e_x^2 v\theta + c\theta & e_y s\theta & d_y \\ -e_x s\theta & -e_y s\theta & c\theta & d_z \\ 0 & 0 & 0 & 1 \end{bmatrix} \tag{11}$$

Meanwhile, as shown in Fig. 2, the following equation is workable.

$${}^{\mathrm{sp}}_{\mathrm{M}}\boldsymbol{T} = {}^{0}_{\mathrm{sp}}\boldsymbol{T}^{-1}\,{}^{0}_{\mathrm{M}}\boldsymbol{T} \tag{12}$$

where ${}^{\mathrm{sp}}_{\mathrm{M}}\boldsymbol{T}$ is the transformation matrix from frame {M} to frame {sp}.

The transformation matrix ${}^{\mathrm{sp}}_{\mathrm{M}}\boldsymbol{T}$ can be obtained by substituting Eq. (2) into Eq. (12).

$${}^{\mathrm{sp}}_{\mathrm{M}}\boldsymbol{T} = \begin{bmatrix} t_{11}c5 + t_{21}s4s5 - t_{31}c4s5 & t_{12}c5 + t_{22}s4s5 - t_{32}c4s5 & t_{13}c5 + t_{23}s4s5 - t_{33}c4s5 & D_X c5 + D_Y s4s5 - D_Z c4c5 \\ t_{21}c4 + t_{31}s4 & t_{22}c4 + t_{32}s4 & t_{23}c4 + t_{33}s4 & D_Y c4 + D_Z s4 \\ t_{11}s5 - t_{21}s4c5 + t_{31}c4c5 & t_{12}s5 - t_{22}s4c5 + t_{32}c4c5 & t_{13}s5 - t_{23}s4c5 + t_{33}c4c5 & D_X s5 - D_Y s4c5 + D_Z c4c5 - z_{\mathrm{sp}} - z_7 \\ 0 & 0 & 0 & 1 \end{bmatrix} \tag{13}$$

where

$$\begin{aligned} t_{11} &= e_y^2 v\theta + c\theta,\ t_{12} = -e_x e_y v\theta,\ t_{13} = e_x s\theta \\ t_{21} &= -e_x e_y v\theta,\ t_{22} = e_x^2 v\theta + c\theta,\ t_{23} = e_y s\theta \\ t_{31} &= -e_x s\theta,\ t_{32} = -e_y s\theta,\ t_{33} = c\theta \\ D_X &= d_x - x_1 - x_2 - x_3 - x_4 \\ D_Y &= d_y - y_1 - y_2 - y_3 - y_4 \\ D_Z &= d_z - z_1 - z_2 - z_3 - z_4 \end{aligned}$$

When the spindle is regulated to coincide with the normal vector, a matrix equation is expressed as

$${}^{\mathrm{sp}}_{\mathrm{M}}\boldsymbol{T} = \boldsymbol{I}_{4\times 4} \tag{14}$$

The new orientation of the end-effector normal reorientation unit and the new position of the robot main body position regulation unit are obtained from Eq. (14) as

$$\left.\begin{aligned} \theta_4 &= \tan^{-1}\left(-e_y\sqrt{\frac{1-e_z}{1+e_z}}\right) \\ \theta_5 &= \tan^{-1}\left(\frac{e_x((e_x^2+e_y^2)(1-e_z)+e_z)\sqrt{1-e_z^2}}{e_x^2 e_z - 2e_z - e_x^2 - 1}\right) \\ x_1 &= d_x - x_2 - x_3 - x_4 - D_X \\ y_2 &= d_y - y_1 - y_3 - y_4 - D_Y \\ z_3 &= d_z - z_1 - z_2 - z_4 - D_Z \end{aligned}\right\} \tag{15}$$

with

$$D_X = \frac{(z_{\mathrm{sp}} + z_7)(\cos\theta_4\cos\theta_5 + \tan\theta_4\sin\theta_5)}{\tan\theta_4\sin\theta_4 + \cos\theta_4\cos\theta_5(\sin\theta_5 + \cos\theta_5)}$$

$$D_Y = \frac{-(z_{\mathrm{sp}} + z_7)\tan\theta_4\cos\theta_5}{\tan\theta_4\sin\theta_4 + \cos\theta_4\cos\theta_5(\sin\theta_5 + \cos\theta_5)}$$

$$D_Z = \frac{(z_{\mathrm{sp}} + z_7)\cos\theta_5}{\tan\theta_4\sin\theta_4 + \cos\theta_4\cos\theta_5(\sin\theta_5 + \cos\theta_5)}$$

Hence, the rotational angles of the two axes of the end-effector reorientation unit and the displacements of the three axes of the robot main body are obtained from Eq. (15) as

$$\left.\begin{aligned} \Delta\theta_4 &= \theta_4 - \theta_4' \\ \Delta\theta_5 &= \theta_5 - \theta_5' \\ \Delta x_1 &= x_1 - x_1' \\ \Delta y_2 &= y_2 - y_2' \\ \Delta z_3 &= z_3 - z_3' \end{aligned}\right\} \tag{16}$$

where θ_4' and θ_5' represent the original angles of the end-effector reorientation unit before reorientation, and x_1', y_2' and z'_3 are the original positions of the robot main body before regulation, respectively.

3 Reorientation Algorithm Simulation

The arrangement of four displacement sensors around a spindle is shown in Fig. 4, where the deflection angle θ is used to avoid the unsolvable case of Eq. (4). In this paper, the value of θ is set to 10°. A device is set which can rearrange the sensors to avoid the case that the normal vector cannot be measured or calculated. And a is the distance between two sensors, $a = 40$ mm.

On the XY plane in the base frame {0}, the coordinate of the drilling point is $M(x_{\mathrm{m}}, y_{\mathrm{m}})$ and the coordinates of the four displacement sensors are $S_i(x_{si}, y_{si})$ ($i = 1, 2, 3, 4$). Thus the relationships between them are expressed as

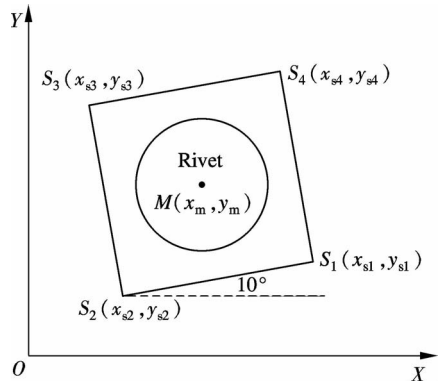

Fig. 4 Displacement sensor arrangement around the spindle

$$\begin{bmatrix} x_{s1} \\ y_{s1} \\ 1 \end{bmatrix} = \begin{bmatrix} \cos\theta & -\sin\theta & x_m \\ \sin\theta & \cos\theta & y_m \\ 0 & 0 & 1 \end{bmatrix} \begin{bmatrix} a/2 \\ -a/2 \\ 1 \end{bmatrix} \tag{17}$$

$$\begin{bmatrix} x_{s2} \\ y_{s2} \\ 1 \end{bmatrix} = \begin{bmatrix} \cos\theta & -\sin\theta & x_m \\ \sin\theta & \cos\theta & y_m \\ 0 & 0 & 1 \end{bmatrix} \begin{bmatrix} -a/2 \\ -a/2 \\ 1 \end{bmatrix} \tag{18}$$

$$\begin{bmatrix} x_{s3} \\ y_{s3} \\ 1 \end{bmatrix} = \begin{bmatrix} \cos\theta & -\sin\theta & x_m \\ \sin\theta & \cos\theta & y_m \\ 0 & 0 & 1 \end{bmatrix} \begin{bmatrix} -a/2 \\ a/2 \\ 1 \end{bmatrix} \tag{19}$$

$$\begin{bmatrix} x_{s4} \\ y_{s4} \\ 1 \end{bmatrix} = \begin{bmatrix} \cos\theta & -\sin\theta & x_m \\ \sin\theta & \cos\theta & y_m \\ 0 & 0 & 1 \end{bmatrix} \begin{bmatrix} a/2 \\ a/2 \\ 1 \end{bmatrix} \tag{20}$$

Considering that the measure error of the sensors is $\pm 0.6\%$, simulations are performed with two kinds of curve surfaces as: parabolic surface and a hyperboloid.

The equation of a parabolic surface for simulation is expressed as

$$z = 10 - 0.003y^2 \tag{21}$$

A curve surface expressed by Eq. (21) parallels to the x axis so that the normal vectors to the curve surface parallel along the x axis, and thus the angle errors between the calculated normal vectors and the measured ones are the same along the x axis. If θ, as shown in Fig. 4, is set to 0°, the divisor of Eq. (5) will be zero by substituting the four coordinates calculated by Eqs. (17) to (20) into Eq. (5), so that we cannot measure and calculate the normal vector. So, θ is set to a certain value to ensure that Eq. (4) have unique solution. Without loss of generality, θ is set to 10° in this paper.

Eq. (21) can be rewritten as

$$F(x, y, z) = 0.003y^2 + z - 10 \tag{22}$$

The theoretical vector normal to the parabolic surface expressed by Eq. (22) at the point ${}^0\boldsymbol{D} = [d_x \quad d_y \quad d_z]^T$ is given as

$${}^0\boldsymbol{N}_{\text{theory}} = \left[\frac{\partial F}{\partial x} \quad \frac{\partial F}{\partial y} \quad \frac{\partial F}{\partial z}\right]^T \Big|_{({}^0\boldsymbol{D})} \tag{23}$$

Substituting Eq. (22) to Eq. (23), we obtain

$${}^0\boldsymbol{N}_{\text{theory}} = [0 \quad 0.006y \quad 1]^T \tag{24}$$

The errors between the angles calculated by Eq. (6) and the ones by Eq. (24) are shown in Fig. 5. From Fig. 5, the simulation results with a parabolic surface indicate that the errors between the theoretical value and the calculated value by the algorithm are less than 0.05° within a small region, whereas they are 0.01° in other region.

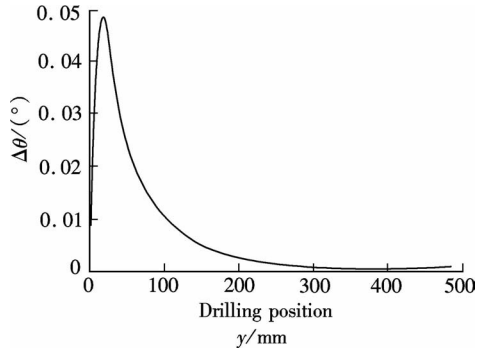

Fig. 5 Angle measurement error of parabolic surface

The equation of a hyperboloid for simulation is expressed as

$$\frac{y^2}{200^2} + \frac{z^2}{50^2} - \frac{x^2}{400^2} = 1 \tag{25}$$

The theoretical vector normal to the hyperboloid expressed by Eq. (25) at the point ${}^0\boldsymbol{D} = [d_x \quad d_y \quad d_z]^T$ is given as

$${}^0N_{\text{theory}} = \left[\frac{2x}{400^2} \quad -\frac{2y}{200^2} \quad -\frac{2z}{50^2}\right]^T \Big|_{({}^0D)} \tag{26}$$

The errors between the angles calculated by Eq. (6) and the ones by Eq. (26) are shown in Fig. 6. From Fig. 6, the simulation results with a hyperboloid indicate that the errors between the theoretical value and the calculated one by the algorithm are less than 0.2° in the whole region.

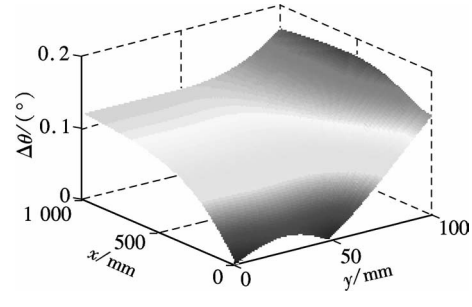

Fig. 6 Angle measurement error of hyperboloid

4 Conclusion

In this paper, a novel algorithm for the regulation of normal orientation and the position of the designed end-effector of a flexible drilling robot is presented. The algo-

rithm measures and calculates the normal vector to the curve surface of a workpiece at the drilling point by four displacement sensors.

The angle error indicated in the product specifications of the end-effector of a flex track drilling robot developed by Electroimpact is less than 0.3°. So the measurement principle and the algorithm can satisfy the practical demands for the regulation of the end-effector of a flexible drilling robot.

References

[1] Millar A, Kihlman H. Reconfigurable flexible tooling for aerospace wing assembly [C]//*Proceedings of the SAE* 2009 *AeroTech Congress and Exhibition*. Seattle, WA, USA, 2009: 013243.

[2] Zhou Wanyong, Zou Fang. Research on automatic drill with five axes for flexible assembly of aircraft wing components [J]. *Aeronautical Manufacturing Technology*, 2010(2): 44 - 46. (in Chinese)

[3] Hogan C, Hartmann J, Thayer B, et al. Automated wing drilling system for the A380-GRAWDE [C]//*Proceedings of the Automated Fastening Conference and Exposition*. Montreal, Canada, 2003: 012940.

[4] Atkinson J, Hartmann J, Jones S, et al. Robotic drilling system for 737 aileron [C]//*Proceedings of the SAE* 2007 *AeroTech Congress and Exhibition*. Los Angeles, CA, USA, 2007: 013821.

[5] Hempstead B, Thayer B, Williams S. Composite automatic wing drilling equipment (CAWDE) [C]//*Aerospace Manufacturing and Automated Fastening Conference and Exhibition*. Toulouse, France, 2006: 013162.

[6] Buttrick J. Flex track drill [J]. *SAE Transactions*, 2003, **112**(1): 389 - 392.

[7] Du Baorui, Feng Ziming. Robot drilling system for automatic drilling of aircraft component [J]. *Aeronautical Manufacturing Technology*, 2010(2): 47 - 50. (in Chinese)

[8] Thompson P, Hartmann J, Feikert E, et al. Flex track for use in production [J]. *SAE Transactions*, 2005, **114**(1): 1039 - 1045.

[9] DeVlieg R, Sitton K, Feikert E, et al. ONCE (one-sided cell end-effector) robotic drilling system [C]//2002 *SAE Automated Fastening Conference and Exhibition*. Chester, Engla, 2002: 012626.

[10] Qin X S, Wang W D, Lou A L, et al. Three-point bracket regulation algorithm for drilling and riveting of aerofoil [J]. *Acta Aeronautica et Astronautica Sinica*, 2007, **28**(6): 1455 - 1460.

[11] Craig J J. *Introduction to robotics mechanics & control* [M]. Addison-Wesley Publishing Company, 1986: 120 - 121.

曲面柔性制孔机器人末端执行器及其法向姿态调整的一种新算法

张来喜　　王兴松

(东南大学机械工程学院,南京 211189)

摘要:设计了一种曲面柔性制孔机器人末端执行器,并针对该末端执行器提出了一种法向姿态调整的新算法. 空间不共面四点可以确定一个与之相切的球面,求出该球面的半径及球心位置,以该球面近似代表制孔点区域的曲面,联结制孔点与该球面球心的矢量即可近似代表制孔点曲面的法矢量. 根据这一原理,该算法首先用4个位移传感器测量出曲面上制孔区域内4个点的坐标,并由此计算出制孔位置的法向矢量,然后计算出此法向矢量与末端执行器上电主轴的轴线矢量的误差. 根据该误差,进一步计算出末端执行器上2个旋转轴的旋转角度及制孔机器人另外3个直线移动方向的移动距离,从而实现调整主轴在制孔点与曲面垂直的功能. 针对2种类型曲面的仿真结果表明,根据该算法可以实现较高的调整精度和效率.

关键词:四点位置调整;末端执行器;柔性制孔机器人;曲面制孔

中图分类号:TP249